Centrum voor Wiskunde en Informatica

REPORT*RAPPORT*

MAS

Modelling, Analysis and Simulation

Modelling, Analysis and Simulation

Riemann-problem and level-set approaches for two-fluid flow computations
II. Fixes for solution errors near interfaces

B. Koren, M.R. Lewis, E.H. van Brummelen, B. van Leer

REPORT MAS-R0113 AUGUST 2001

CWI is the National Research Institute for Mathematics and Computer Science. It is sponsored by the Netherlands Organization for Scientific Research (NWO).
CWI is a founding member of ERCIM, the European Research Consortium for Informatics and Mathematics.

CWI's research has a theme-oriented structure and is grouped into four clusters. Listed below are the names of the clusters and in parentheses their acronyms.

Probability, Networks and Algorithms (PNA)

Software Engineering (SEN)

Modelling, Analysis and Simulation (MAS)

Information Systems (INS)

P.O. Box 94079, 1090 GB Amsterdam (NL)
Kruislaan 413, 1098 SJ Amsterdam (NL)
Telephone +31 20 592 9333
Telefax +31 20 592 4199

ISSN 1386-3703

Riemann-Problem and Level-Set Approaches for Two-Fluid Flow Computations II. Fixes for Solution Errors near Interfaces

B. Koren, M.R. Lewis and E.H. van Brummelen
CWI
P.O. Box 94079, 1090 GB Amsterdam, The Netherlands

B. van Leer
The University of Michigan, Department of Aerospace Engineering
Ann Arbor, MI 48109-2140, USA

ABSTRACT

Fixes are presented for the solution errors ('pressure oscillations') that may occur near two-fluid interfaces when applying a capturing method. The fixes are analyzed and tested. For two-fluid flows with arbitrarily large density ratios, a variant of the ghost-fluid method appears to be a perfect remedy. Results are presented for compressible water-air flows. The results are promising for a further elaboration of this important application area. The paper contributes to the state-of-the-art in computing two-fluid flows.

2000 Mathematics Subject Classification: 65M12, 65M15, 65M60, 76N99, 76T10
Keywords and Phrases: free surfaces, compressible liquid-gas flows, interface capturing, Godunov scheme, level-set method, interface pressure error, ghost-fluid method.
Note: This research was supported by the Dutch Technology Foundation STW (applied science division of NWO and the technology programme of the Ministry of Economic Affairs) and by the Maritime Research Institute Netherlands. The work was carried out under CWI-project MAS2.1 "Computational Fluid Dynamics".

1. Introduction

A known difficulty of capturing contact discontinuities in a conservative formulation of, e.g., the Euler equations is that large solution errors (in literature often referred to as 'pressure oscillations') may arise near the contact discontinuity. (For tracking and fitting approaches the problem does not exist.) We will show that the solution error referred to is proportional to the density ratio. For large density jumps across the interface, the errors may even degenerate to instabilities. Fixes for this solution-error problem are available. We refer to the works of Karni [1, 2] and Abgrall [3], their common paper [4], and also to [5, 6, 7]. In most of the available capturing literature though, the ratio of the two densities at the interface is $\mathcal{O}(1)$–$\mathcal{O}(10^2)$. To our knowledge, only in [5, 6] ratios of $\mathcal{O}(10^3)$, typical water-air ratios, are considered.

Conservative capturing through the two-fluid, linearized Godunov scheme proposed in our foregoing paper [8] also suffers from the problem. In the present paper, we will show this on the basis of a model flow with known exact solution. Flows with a single spatial dimension only are considered. The spatial simplicity allows us to compute fluid-flow problems with known exact solutions.

The contents of the paper is the following. In Section 2, we analyze the solution-error problem near interfaces. Next, in Section 3, some approaches to fix the problem are described. Not all of these approaches (some of them already known) appear to work for water-air flow with its large density jump. One fix is proposed which works perfectly, it is a simple variant of the ghost-fluid method [6]. In Section 4, numerical results are presented for compressible water-air flows.

2. Error near interface

2.1 Fluid-flow equations

To describe a 1D two-fluid (water-air) flow, consider (for a sufficiently small control volume Ω) the following system of equations:

$$\int_\Omega \frac{d}{dt} \begin{pmatrix} \rho \\ \rho u \\ \rho\phi \end{pmatrix} dx + \begin{pmatrix} \rho u \\ \rho u^2 + p \\ \rho u \phi \end{pmatrix}_{\partial\Omega_{right}} - \begin{pmatrix} \rho u \\ \rho u^2 + p \\ \rho u \phi \end{pmatrix}_{\partial\Omega_{left}} = 0, \tag{2.1a}$$

with ρ the bulk density, which is defined as

$$\rho = \alpha(\phi)\rho_w(p) + (1 - \alpha(\phi))\rho_a(p), \tag{2.1b}$$

where α is the volume-of-water fraction, ϕ the level-set function, and where $\rho_w(p)$ and $\rho_a(p)$ are the equations of state for water and air, respectively. For the latter, we use Tait's:

$$\rho_w(p) = \left(\frac{p + B_w p_\infty}{(1 + B_w)p_\infty} \right)^{\frac{1}{\gamma_w}} (\rho_w)_\infty, \quad \rho_a(p) = \left(\frac{p + B_a p_\infty}{(1 + B_a)p_\infty} \right)^{\frac{1}{\gamma_a}} (\rho_a)_\infty. \tag{2.1c}$$

The level-set function ϕ is defined as the signed-distance function and is taken positive in water. For a further discussion of this flow model, see Section 2 in [8].

2.2 Analysis for model flow

Consider a 1D tube with unit length, $x \in [0, 1]$, inflow at $x = 0$, outflow at $x = 1$ and with as initial solution:

$$u(x, t = 0) = U > 0, \tag{2.2a}$$

$$p(x, t = 0) = P, \tag{2.2b}$$

$$\rho(x, t = 0) = \begin{cases} \rho_w(P), & x \le (x_{fs})_{t=0}, \\ \rho_a(P), & x \ge (x_{fs})_{t=0}, \end{cases} \tag{2.2c}$$

where U and P are constant, and where x_{fs} is the location of the free surface, the water-air interface. For $t > 0$, the corresponding exact Euler-flow solution simply reads $u(x, t) = U$, $p(x, t) = P$, $\rho(x, t) = \rho_w(P)$ for $x \le (x_{fs})_{t=0} + Ut$ and $\rho(x, t) = \rho_a(P)$ for $x \ge (x_{fs})_{t=0} + Ut$ (Figure 1). The model flow seems trivial, but it is not. It precisely uncovers the deficiency of capturing methods with regard to material interfaces. For the problem at hand, for the space discretization of (2.1a) we consider an

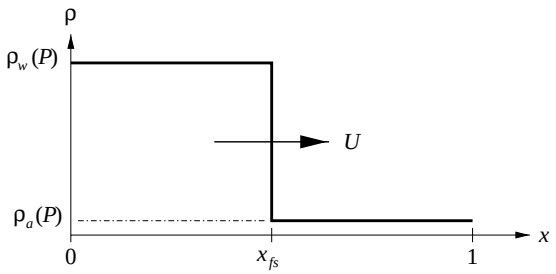

Figure 1: Water-air interface running from left to right through a 1D tube, at constant speed U and pressure P.

equidistant finite-volume grid with mesh size h. For the time integration, just for convenience, we take the forward Euler scheme. The space discretization is taken first-order accurate. Then, denoting the solution in cell i at the old time level by q_i^n, $q = (\rho, \rho u, \rho\phi)^T$, we have as equation for the solution q_i^{n+1} at the new time level:

$$q_i^{n+1} = q_i^n - \frac{\Delta t}{h}\left(F(q_i^n, q_{i+1}^n) - F(q_{i-1}^n, q_i^n)\right), \tag{2.3}$$

with Δt the time step, and with F denoting the two-fluid, linearized Godunov flux (3.11)–(3.12) from [8]. Considering the situation where q_{i-1}^n, q_i^n and q_{i+1}^n are according to initial solution (2.2), with $(x_{fs})^n = (x_{fs})_{t=0} = x_{i-\frac{1}{2}}$ (Figure 2), with the two-fluid, linearized Godunov scheme presented in [8] we get

$$\rho_i^{n+1} = \sigma\rho_w + (1-\sigma)\rho_a, \tag{2.4a}$$

$$(\rho u)_i^{n+1} = (\sigma\rho_w + (1-\sigma)\rho_a)\, U, \tag{2.4b}$$

$$(\rho\phi)_i^{n+1} = (\sigma\rho_w - (1-\sigma)\rho_a)\,\frac{h}{2}, \tag{2.4c}$$

where $\sigma \equiv \frac{U\Delta t}{h}$.

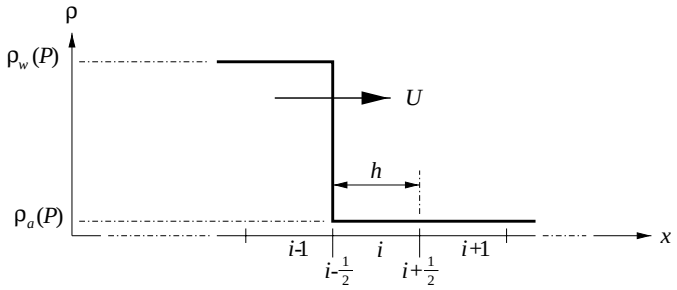

Figure 2: Bulk density distribution near cell i at time level n, water-air interface at $x_{i-\frac{1}{2}}$.

Note that ρ_i^{n+1} according to (2.4) is exact, as is $u_i^{n+1} = \frac{(\rho u)_i^{n+1}}{\rho_i^{n+1}} = U$. However, for ϕ_i^{n+1} it follows from (2.4)

$$\phi_i^{n+1} = \frac{(\rho\phi)_i^{n+1}}{\rho_i^{n+1}} = \frac{\sigma\rho_w - (1-\sigma)\rho_a}{\sigma\rho_w + (1-\sigma)\rho_a}\frac{h}{2}, \tag{2.5}$$

whereas the exact discrete solution reads $(\phi_i^{n+1})_{exact} = -\frac{h}{2} + \sigma h$. Hence, for the local discretization error $\Delta\phi_i^{n+1} = \phi_i^{n+1} - \left(\phi_i^{n+1}\right)_{exact}$ it holds

$$\Delta\phi_i^{n+1} = \sigma(1-\sigma)\frac{\rho_w - \rho_a}{\sigma\rho_w + (1-\sigma)\rho_a}h. \tag{2.6}$$

So, $\Delta\phi_i^{n+1} = 0$ only if – trivially – $\sigma = 0$, if $\sigma = 1$ (formally unstable with forward Euler and $\sigma \equiv \frac{U\Delta t}{h}$), or if $\rho_w = \rho_a$. For $0 < \sigma < 1$ and $\rho_w > \rho_a$ it always holds $\Delta\phi_i^{n+1} > 0$. The local discretization error (2.6) is $\mathcal{O}(h)$, but can *not* be made of higher order by applying a higher-order discretization. (This holds for any numerical flux function F.) Higher than first-order accuracy is simply inhibited by the

bulk density, which is a smeared out representation of the exact discrete density. Through bulk-density formula

$$\rho(\phi,p)=\alpha(\phi)\rho_w(p)+(1-\alpha(\phi))\rho_a(p),\quad \alpha(\phi)\in[0,1], \tag{2.7}$$

with α denoting the volume-of-fluid (water) fraction, the error (2.6) carries over into a pressure error Δp_i^{n+1}. Given $\Delta\rho_i^{n+1}=0$, from (2.7) it follows after linearization $\rho_i^{n+1}=\left(\alpha_i^{n+1}+\Delta\alpha_i^{n+1}\right)\left(\rho_w(P)+\frac{\Delta p_i^{n+1}}{c_w^2(P)}\right)+\left(1-\alpha_i^{n+1}-\Delta\alpha_i^{n+1}\right)\left(\rho_a(P)+\frac{\Delta p_i^{n+1}}{c_a^2(P)}\right)$, i.e.,

$$\Delta p_i^{n+1}=\frac{-c_w^2c_a^2}{\left(\alpha_i^{n+1}+\Delta\alpha_i^{n+1}\right)c_a^2+\left(1-\alpha_i^{n+1}-\Delta\alpha_i^{n+1}\right)c_w^2}(\rho_w-\rho_a)\Delta\alpha_i^{n+1}. \tag{2.8}$$

From the formulae for the volume-of-fluid fraction α_i as given in Section 3.1 of [8], it follows that, besides on $\Delta\phi_i^{n+1}$, $\Delta\alpha_i^{n+1}$ also depends on $\Delta\phi_{i-1}^{n+1}$ and $\Delta\phi_{i+1}^{n+1}$. For the model flow considered, it follows with the two-fluid, linearized Godunov scheme: $\phi_{i-1}^{n+1}=\frac{(\rho\phi)_{i-1}^{n+1}}{\rho_{i-1}^{n+1}}=\frac{h}{2}+\sigma h$ and $\phi_{i+1}^{n+1}=\frac{(\rho\phi)_{i+1}^{n+1}}{\rho_{i+1}^{n+1}}=-\frac{3h}{2}+\sigma h$, which are both the exact results. Resuming, we have $\phi_i^{n+1}=-\frac{h}{2}+\sigma h+\Delta\phi_i^{n+1}$, $\phi_{i-\frac{1}{2}}^{n+1}=\sigma h+\frac{1}{2}\Delta\phi_i^{n+1}$ and $\phi_{i+\frac{1}{2}}^{n+1}=-h+\sigma h+\frac{1}{2}\Delta\phi_i^{n+1}$, with $\Delta\phi_i^{n+1}$ according to (2.6). With the procedure for computing the volume-of-fluid fraction α as described in Section 3.1 of [8], the following expressions can then be derived for the error $\Delta\alpha_i^{n+1}=\alpha_i^{n+1}-\left(\alpha_i^{n+1}\right)_{exact}$:

$$\Delta\alpha_i^{n+1}=\left(\frac{1}{2}+\sigma\right)\frac{\Delta\phi_i^{n+1}}{h-\Delta\phi_i^{n+1}},\quad \phi_i^{n+1}\le 0, \tag{2.9a}$$

$$\Delta\alpha_i^{n+1}=\left(\frac{3}{2}-\sigma\right)\frac{\Delta\phi_i^{n+1}}{h+\Delta\phi_i^{n+1}},\quad \phi_i^{n+1}\ge 0. \tag{2.9b}$$

Note that $\Delta\alpha_i^{n+1}=\mathcal{O}(1)$ (i.e., mesh-size-independent) and – hence – with (2.8) also the pressure error Δp_i^{n+1} is! Also note that the pressure error (2.8) is proportional to the density ratio $\frac{\rho_w}{\rho_a}$. This illustrates the poor, density-ratio-dependent solution-error behavior already mentioned in the beginning of this section. (Note that the error behavior is not so poor that the denominator $h-\Delta\phi_i^{n+1}$ in (2.9a) may become zero for $0<\sigma<1$ and $\rho_w>\rho_a$.)

2.3 Guidelines for error improvements

Before proposing improvements of the poor local error behavior near the interface, it is useful to make an error analysis of bulk-density relation (2.7) and – also – to consider the conservative equations near the interface.

2.3.1 Error analysis of bulk-density relation Errors in the pressure and volume-of-fluid fraction (Δp and $\Delta\alpha$) induce an error in the bulk density ($\Delta\rho$), which, given (2.7), satisfies the equation

$$\rho+\Delta\rho=(\alpha+\Delta\alpha)\rho_w(p+\Delta p)+(1-\alpha-\Delta\alpha)\rho_a(p+\Delta p). \tag{2.10}$$

For the model flow and discretization method considered in Section 2.2, we found $\Delta\rho=0$ and $\Delta\alpha=\mathcal{O}(1)$. Then, according to (2.10), $\Delta p=\mathcal{O}(1)$ as well, which is in agreement with what we derived in Section 2.2. Near the interface, instead of the zeroth-order pressure error Δp described by (2.8)–(2.9), we ideally prefer $\Delta p=0$, which implies according to (2.10)

$$\Delta\rho=\Delta\alpha(\rho_w(p)-\rho_a(p)). \tag{2.11}$$

One of the fixes to be considered in the following is to make the numerical method so that $\Delta\rho$ and $\Delta\alpha$ exactly satisfy (2.11).

2.3.2 Reconsideration of fluid-flow equations near interface Consider the situation in which the interface is in cell $\Omega = \Omega_i$ (*only* the interface, so no shock or rarefaction). Since velocity and pressure are continuous across the interface, for sufficiently small Ω_i, we may then write by good approximation: $u_{i-\frac{1}{2}} = u_{i+\frac{1}{2}} = u_i$ and $p_{i-\frac{1}{2}} = p_{i+\frac{1}{2}}$. With this, (2.1a) can be rewritten as

$$\int_{\Omega_i} \frac{d}{dt} \begin{pmatrix} \rho \\ \rho u \\ \rho\phi \end{pmatrix} dx + u_i \left(\begin{pmatrix} \rho \\ \rho u \\ \rho\phi \end{pmatrix}_{\partial\Omega_{i+\frac{1}{2}}} - \begin{pmatrix} \rho \\ \rho u \\ \rho\phi \end{pmatrix}_{\partial\Omega_{i-\frac{1}{2}}} \right) = 0, \tag{2.12}$$

i.e., as

$$\int_{\Omega_i} \frac{dq}{dt} dx + u_i \left(q_{i+\frac{1}{2}} - q_{i-\frac{1}{2}} \right) = 0, \tag{2.13}$$

which is a system of advection equations for the entire solution vector q_i. (Contact discontinuities are linear phenomena.) If all conservative solution components are advected – ρ_i, $(\rho u)_i$ and $(\rho\phi)_i$ – then any solution component in Ω_i (either conservative or non-conservative) is. I.e., in (2.13), in a cell with (only) a contact discontinuity, instead of the fully conservative solution representation $q_i = (\rho_i, (\rho u)_i, (\rho\phi)_i)$ we may equally well consider, e.g., the partially conservative representation $q_i = (\rho_i, (\rho u)_i, \phi_i)$, the fully non-conservative representation $q_i = (u_i, p_i, \phi_i)$, or whatever. This knowledge is important. In combination with error equation (2.10), it allows us to derive a fix for the zeroth-order error observed in Section 2.2.

3. Fixes for error in cell with interface

3.1 Advection of level-set function

This approach is based on the observation made in Section 2.2 that the update of ϕ_i^n through division of $(\rho\phi)_i^{n+1}$ by ρ_i^{n+1} leads to a first-order accuracy barrier in ϕ_i^{n+1} because of the intrinsic smearing in the bulk-density representation itself. For the update of the real physical quantities ρ_i and $(\rho u)_i$ we may stick to the conservative formulation and, hence, to the two-fluid, linearized Godunov scheme. Doing so, with the forward Euler, first-order upwind discretization of the single advection equation

$$\int_{\Omega_i} \frac{d\phi}{dt} dx + u_i \left(\phi_{i+\frac{1}{2}} - \phi_{i-\frac{1}{2}} \right) = 0, \tag{3.1}$$

for the model flow considered – in addition to (2.4a) and (2.4b) for ρ_i^{n+1} and $(\rho u)_i^{n+1}$ – we get

$$\phi_i^{n+1} = -\frac{h}{2} + \sigma h, \tag{3.2}$$

which is exact. Note that ϕ_i^{n+1} is exact because ϕ has been defined as the signed-distance function. (A nonlinear spatial distribution of ϕ would have yielded an error $\Delta\phi_i^{n+1}$.) Because $\Delta\phi_i^{n+1} = 0$, it also holds $\Delta\alpha_i^{n+1} = 0$. Since $\Delta\rho_i^{n+1} = 0$ as well (Section 2.2), from (2.10) it then follows $\Delta p_i^{n+1} = 0$. In all other cells, the fully conservative scheme (2.3) is applied, yielding there the exact discrete solution. However, at time level $n+2$ the numerical solution is no longer exact. According to the linearized Godunov scheme it holds for first-order state interpolation to the cell faces: $\rho_{i-\frac{1}{2}}^{n+1} = \rho_{i-1}^{n+1} = \rho_w$, $\rho_{i+\frac{1}{2}}^{n+1} = \rho_i^{n+1} = \sigma\rho_w + (1-\sigma)\rho_a$ and $u_{i-\frac{1}{2}}^{n+1} = u_{i+\frac{1}{2}}^{n+1} = U$. Then, from (2.3) it follows $\rho_i^{n+2} = 2\sigma\rho_w + (1-2\sigma)\rho_a - \sigma^2(\rho_w - \rho_a)$, whereas $\left(\rho_i^{n+2}\right)_{exact} = 2\sigma\rho_w + (1-2\sigma)\rho_a$. Hence, $\Delta\rho_i^{n+2} = -\sigma^2(\rho_w - \rho_a)$. With the forward-Euler, first-order upwind discretization of (3.1), it follows $\Delta\phi_i^{n+2} = 0$ and, as a consequence, $\Delta\alpha_i^{n+2} = 0$. With (2.10), it then follows, since $\Delta\rho_i^{n+2} = \mathcal{O}(1)$, that $\Delta p_i^{n+2} = \mathcal{O}(1)$. So, this partially conservative approach is not a fix. With some tricks one can make the method work. Taking for the left and right cell-face densities to be substituted into the linearized Godunov scheme, instead of the *bulk*

densities, the *local (non-bulk)* densities (pure water or pure air) at $t = t^n$, the method works as long as the interface does not cross a cell face during a time step. I.e., the method works for $\sigma = \frac{1}{m}$, with m integer. For the problem at hand, verify that, instead of $\rho_{i+\frac{1}{2}}^{n+1} = \sigma\rho_w + (1-\sigma)\rho_a$, this would have yielded $\rho_{i+\frac{1}{2}}^{n+1} = \rho_a$ (pure air), and so (with $\rho_{i-\frac{1}{2}}^{n+1} = \rho_w$ and $u_{i\pm\frac{1}{2}}^{n+1} = U$): $\rho_i^{n+2} = 2\sigma\rho_w + (1-2\sigma)\rho_a$, thus $\Delta\rho_i^{n+2} = 0$, and – hence – with $\Delta\alpha_i^{n+2} = 0$: $\Delta p_i^{n+2} = 0$, instead of $\Delta p_i^{n+2} = \mathcal{O}(1)$. Aforementioned requirement on σ is too restrictive to let the method be of much practical use.

3.2 Advection of velocity, pressure and level-set function

Taking in (2.13) $q_i = (u_i, p_i, \phi_i)$, with $(u_{i-\frac{1}{2}}, p_{i-\frac{1}{2}}) = (u_{i+\frac{1}{2}}, p_{i+\frac{1}{2}})$, it follows the exact result

$$\begin{pmatrix} u \\ p \\ \phi \end{pmatrix}_i^{n+1} = \begin{pmatrix} u \\ p \\ \phi \end{pmatrix}_i^{n} + \begin{pmatrix} 0 \\ 0 \\ \sigma h \end{pmatrix} = \begin{pmatrix} U \\ P \\ -\frac{h}{2} + \sigma h \end{pmatrix}. \tag{3.3}$$

However, in cell Ω_{i+1} an error arises. Verify that q_{i+1}^{n+1} is still exact, $q_{i+1}^{n+1} = (U, P, -\frac{3}{2}h + \sigma h)$, as is $q_{i+2}^{n+1} = (U, P, -\frac{5}{2}h + \sigma h)$, but for $t = t^{n+2}$ we find with the linearized Godunov scheme: $\rho_{i+1}^{n+2} = \rho_a + \sigma^2(\rho_w - \rho_a)$. For $\sigma < \frac{1}{2}$, this is wrong; water is erroneously transported from cell i into cell $i+1$. The corresponding error reads: $\Delta\rho_i^{n+2} = \sigma^2(\rho_w - \rho_a) = \mathcal{O}(1)$. Meanwhile, for $\sigma < \frac{1}{2}$ such that $\phi_{i+\frac{1}{2}}^{n+2} = \phi_{i+\frac{3}{2}}^{n+2}$ are both still negative, we correctly find $\alpha_{i+1}^{n+2} = 0$. So, with (2.10) it then follows $\Delta p_{i+1}^{n+2} = \mathcal{O}(1)$ and therefore this approach – although (trivially) fixing the pressure-error problem in the cell with interface – is not (yet) good either, because it yields an error in a neighboring cell.

3.3 Advection of density and volume-of-fluid fraction

In Section 2.3 we have seen that if $\Delta\rho$ and $\Delta\alpha$ are such that (2.11) is satisfied, then $\Delta p = 0$. We derive a possible fix which is based on (2.11). On the basis of general advection equation (2.13), we can directly write the advection equations

$$\int_{\Omega_i} \frac{d\rho}{dt} dx + u_i \left(\rho_{i+\frac{1}{2}} - \rho_{i-\frac{1}{2}}\right) = 0, \tag{3.4a}$$

$$\int_{\Omega_i} \frac{d\alpha}{dt} dx + u_i \left(\alpha_{i+\frac{1}{2}} - \alpha_{i-\frac{1}{2}}\right) = 0. \tag{3.4b}$$

The peculiar cell-face based volume-of-fluid fractions $\alpha_{i-\frac{1}{2}}$ and $\alpha_{i+\frac{1}{2}}$ in (3.4b) may become functions of real volume-of-fluid fractions upon further discretization. Yet, further discretization is not necessary since (3.4a) and (3.4b) are identical. 'Extension' of the relation $p_{i-\frac{1}{2}} = p_{i+\frac{1}{2}}$, which underlies (2.13), to $p_{i-\frac{1}{2}} = p_{i+\frac{1}{2}} = p_i$ implies that with $\rho = \alpha\rho_w(p) + (1-\alpha)\rho_a(p)$, (3.4a) can be rewritten as (3.4b). So, when we maintain (3.4a), the updates $(\rho_i^{n+1} - \rho_i^n)$, $(\rho_i^{n+2} - \rho_i^{n+1})$, etc. which it renders, may be directly translated (through (2.11)) into updates $(\alpha_i^{n+1} - \alpha_i^n)$, $(\alpha_i^{n+2} - \alpha_i^{n+1})$, etc. Whereas in the previous fix the pressure error was explicitly set to zero, here it is implicitly done so. However, as with the fully non-conservative approach from Section 3.2, in the second time step an $\mathcal{O}(1)$ pressure error arises in neighboring cell Ω_{i+1}, when the fully conservative approach is still applied there. Moreover, even in a better case, this fix will yield an exact pressure solution at the expense of a diffused density profile. A perfect fix is a variant of the so-called ghost-fluid method [6]. The variant is described in the next section.

3.4 Ghost-fluid method

In [6], the ghost-fluid method is introduced for the non-homentropic Euler equations of gas dynamics. For our more compact system of fluid-flow equations, we propose a simple variant of the ghost-fluid

method. As the so-called ghost cells we define those cells in which there is an interface (i.e., a zero of the level-set function). These cells are considered in an ambiguous manner: as fully filled with water (ghost water) and as fully filled with air (ghost air). Then, still considering the 1D situation for convenience, across the two walls of the ghost cell, both water and air fluxes of mass and momentum are computed (ghost fluxes). On the basis of the difference between the two ghost-water fluxes, the ghost-water solution is updated (i.e., its mass and momentum). Likewise, the ghost-air solution is. Expressed in (u,p)-variables, these two new ghost solutions (for water and air) will generally not differ very much. (For the 1D problem introduced in Section 2.2, both solutions will be even identical.) Throughout the entire computational domain the level-set function is simply advected with (3.1). In case the updated ghost-water and ghost-air solutions do differ, we propose the following. From the (updated) level-set solution, the volume-of-fluid fraction in the ghost cell can be computed. Then, the solution in the ghost cell is made unique with

$$\begin{pmatrix} u \\ p \end{pmatrix} = \alpha \begin{pmatrix} u_w \\ p_w \end{pmatrix} + (1-\alpha) \begin{pmatrix} u_a \\ p_a \end{pmatrix}. \tag{3.5}$$

There are no physical or mathematical arguments for applying this weighting, other choices are possible. The fluxes (real and ghost) are computed with the single-fluid version of the two-fluid, linearized Godunov scheme. To compute a water flux (either real or ghost), in the expressions for $u_{\frac{1}{2}}$ and $p_{\frac{1}{2}}$ (given in Section 3.3 of [8]), for ρ_0, ρ_1, c_0 and c_1 the water values are taken. The similar is done for the computation of the air fluxes. Note that in the computation of all types of fluxes (real or ghost, water or air), use is made of the same, unique values of u and p in each cell. This uniqueness ensures that the free-surface conditions are satisfied implicitly. In [6], for the non-homentropic Euler equations of gas dynamics, entropy is extrapolated across the interface. The present homentropic equations do not require any solution-component extrapolation. Tangential velocity components do not yet apply here. In multi-D, in each cell, besides the physical normal velocity component and pressure, we would also use the physical tangential velocity components available there. (With Navier-Stokes as the ultimate flow model, like the normal velocity component and pressure, the tangential velocity components will also be continuous across the interface.) Considering the 1D situation with, at time $t = t^n$, the interface somewhere in cell i, with – say – water at the left, in case of the first-order accurate space discretization, the fluxes to be computed are those depicted in Figure 3. So, only across the cell faces $i - \frac{1}{2}$ and $i + \frac{1}{2}$ ghost-water and ghost-air fluxes are computed, across all cell faces left of cell face $i - \frac{1}{2}$: real water fluxes and across all cell faces right of $i + \frac{1}{2}$: real air fluxes.

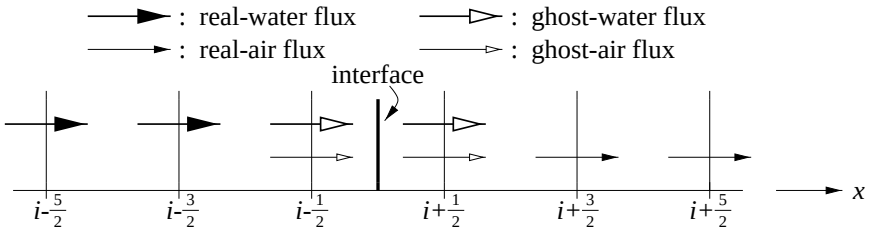

Figure 3: Types of fluxes computed in present ghost-fluid method.

Note that in the ghost-fluid method the interface is no longer captured at the smallest discrete level (that of a cell face), but at the next larger: a cell. Because in the ghost-fluid method fluxes are always of the single-fluid type, explicit calculation of $u_{\frac{1}{2}}$ and $p_{\frac{1}{2}}$ can be done by using, e.g., Osher's scheme, instead of the linearized Godunov scheme.

4. Numerical results

4.1 Water front at constant speed and pressure

4.1.1 Numerical choices The first test case to be considered is the 1D tube flow already introduced in Section 2.2. Numerical values to be considered are: $(x_{fs})_{t=0} = 0.5$ (initial interface halfway tube) or $(x_{fs})_{t=0} = 0$ (initial interface at inlet boundary), $U = 1$, $P = 1$, $\rho_w(P) = 1$, $\rho_a(P) = 0.001$ (in the ideal case), $\gamma_w = 7$, $\gamma_a = \frac{7}{5}$, $B_w = 3000$ and $B_a = 0$. According to the speed-of-sound relations

$$c_w^2 = \gamma_w \frac{(1 + B_w)p}{\rho_w}, \tag{4.1a}$$

$$c_a^2 = \gamma_a \frac{p}{\rho_a}, \tag{4.1b}$$

these values imply $c_w(P) \approx \sqrt{15}\, c_a(P)$, which agrees fairly well with common sea-level conditions. As in Section 2, the grids to be used are equidistant. The boundary conditions to be imposed are $u(x = 0, t) = U > 0$, $\phi(x = 0, t) = Ut$ and $p(x = 1, t) = P$. Time integration is done with the forward Euler scheme, with the time step constant and sufficiently small to guarantee stability:

$$\Delta t = \sigma \frac{h}{U + c_w(P)}, \quad \sigma < 1. \tag{4.2}$$

The space discretization is taken first-order accurate, like in Section 2.2.

4.1.2 Results fully conservative approach This is the approach without any fixes for solution errors near the interface. For the numerical values just mentioned, the computation breaks down. Stumbling block is the large density ratio. In Figure 4, pressure errors are depicted for computations with successively the following three still rather small density ratios: $\frac{\rho_w}{\rho_a} = 2, 4$ and 8, and after the following three numbers of time steps: 10 (left column of graphs), 20 (middle column of graphs) and 40 (right column). The time step on the coarsest grid is twice as large as that on the middle grid and four times larger than that on the finest grid. So, note that in each of the eight graphs (no results were obtained for $\frac{\rho_w}{\rho_a} = 8$ and 40 time steps), the three pressure-error distributions correspond with the same number of time steps (10, 20 or 40), *not* with the same time. The pressure error appears to be about linearly proportional to the number of time steps taken. In agreement with the theoretical findings, it also increases with the density ratio $\frac{\rho_w}{\rho_a}$. The latter increase is clearly nonlinear. With the conservative approach, results for $\frac{\rho_w}{\rho_a} = 1000$ are still far out of reach. The deceptive performance of the conservative approach was expected given the analytical results of Section 2.2.

4.1.3 Results advection of level-set function Here the fix proposed in Section 3.1 is numerically investigated. The fix is applied not only in the cell in which the interface actually is, but also in its left and right neighbor cell. The fix clearly gives an improvement as compared to the fully conservative approach, but the fix is not adequate. For $(x_{fs})_{t=0} = 0$ and $\frac{\rho_w}{\rho_a} = 10$, in each of the three graphs in Figure 5 we present the computed bulk-density profiles at $t = 0.0, 0.1, 0.2, \ldots, 1.0$. The results look perfect, but they are not. They are cursed with a pressure error, which for $\frac{\rho_w}{\rho_a} = 10$ is still negligibly small. But, as in the previous section, the error grows rapidly with increasing density ratio $\frac{\rho_w}{\rho_a}$. Results similar to those in Figure 5 cannot be obtained for $\frac{\rho_w}{\rho_a} = 1000$, not even for $\frac{\rho_w}{\rho_a} = 100$. From Figure 6 it appears that the pressure error grows exponentially with $\frac{\rho_w}{\rho_a}$.

4.1.4 Results advection of velocity, pressure and level-set function Here, the fix proposed in Section 3.2 is tested. The advection of u, p and ϕ is applied in the cell with interface as well as in its left and right neighboring cell. The fix is an improvement compared to that with advection of ϕ only, but it does not work satisfactorily either. It also breaks down for increasing density ratio $\frac{\rho_w}{\rho_a}$; for $\frac{\rho_w}{\rho_a} = 100$ after $t = 0.7$, and for $\frac{\rho_w}{\rho_a} = 1000$ after $t = 0.4$ (Figure 7).

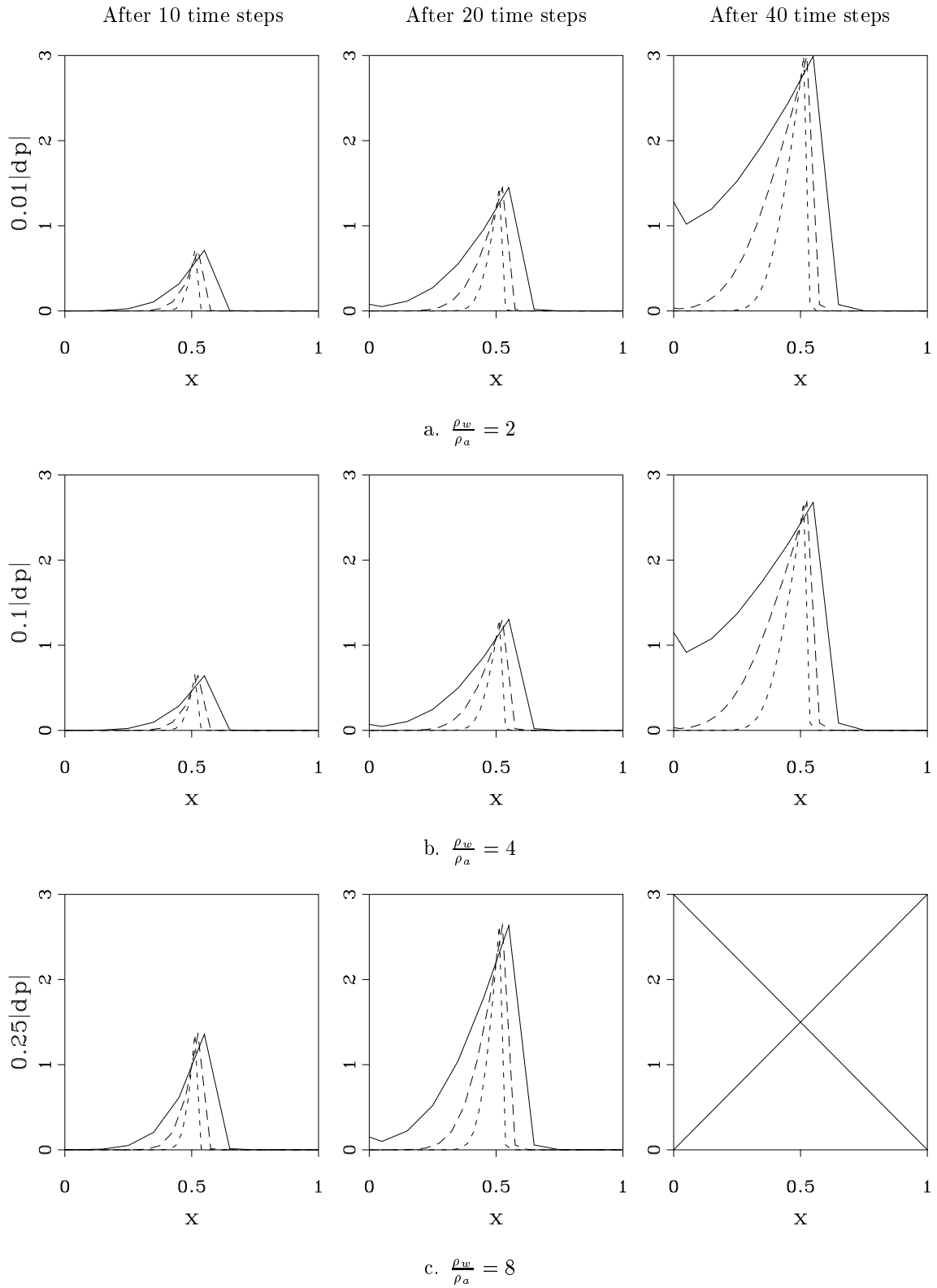

a. $\frac{\rho_w}{\rho_a} = 2$

b. $\frac{\rho_w}{\rho_a} = 4$

c. $\frac{\rho_w}{\rho_a} = 8$

Figure 4: Pressure-error distributions fully conservative approach (solid lines: $h = \frac{1}{10}$, coarsely dashed lines: $h = \frac{1}{20}$, finely dashed lines: $h = \frac{1}{40}$).

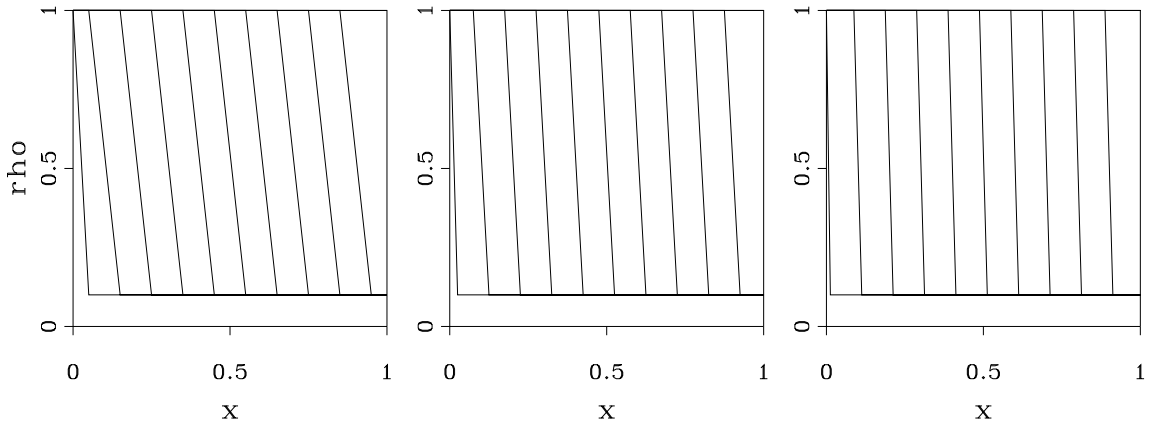

a. $h = \frac{1}{10}$ b. $h = \frac{1}{20}$ c. $h = \frac{1}{40}$

Figure 5: Bulk-density profiles at $t = 0.0, 0.1, 0.2, \ldots, 1.0$, fix with advection of level-set function, $\frac{\rho_w}{\rho_a} = 10$.

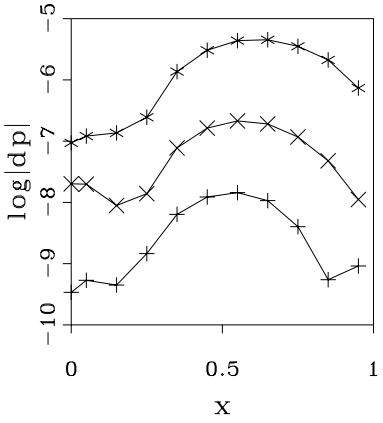

Figure 6: Pressure-error distributions at $t = 0.1$ for $\frac{\rho_w}{\rho_a} = 70\,(+),\ 75\,(\times)$ and $80\,(*)$, fix with advection of level-set function, $h = \frac{1}{40}$.

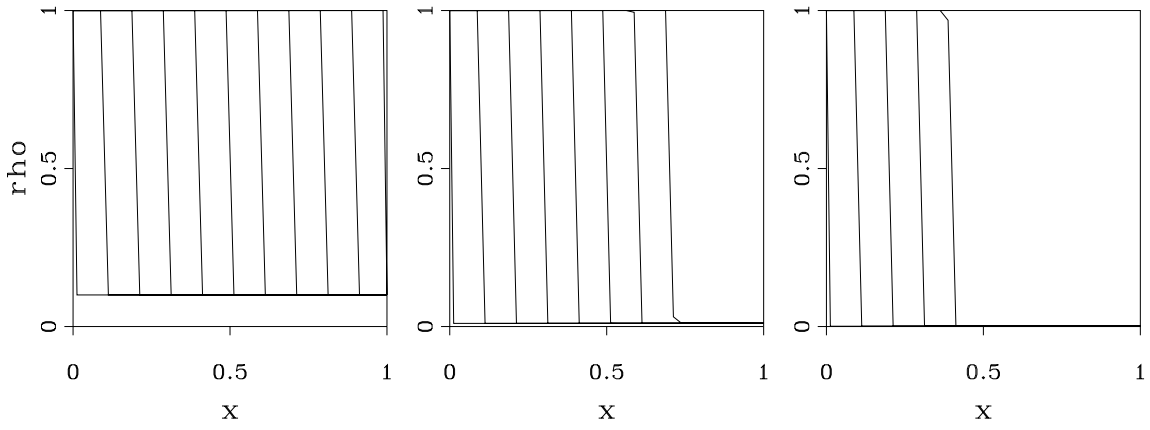

a. $\frac{\rho_w}{\rho_a} = 10$ b. $\frac{\rho_w}{\rho_a} = 100$ c. $\frac{\rho_w}{\rho_a} = 1000$

Figure 7: Bulk-density profiles at $t = 0.0, 0.1, 0.2, \ldots, 1.0$, fix with advection of velocity, pressure and level-set function, $h = \frac{1}{40}$.

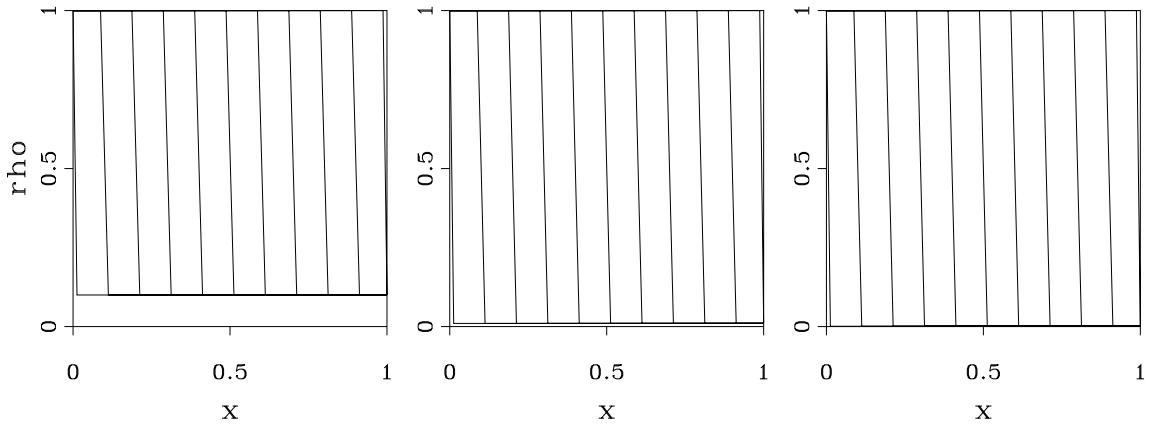

a. $\frac{\rho_w}{\rho_a} = 10$ b. $\frac{\rho_w}{\rho_a} = 100$ c. $\frac{\rho_w}{\rho_a} = 1000$

Figure 8: Bulk-density profiles at $t = 0.0, 0.1, 0.2, \ldots, 1.0$, ghost-fluid method, $h = \frac{1}{40}$.

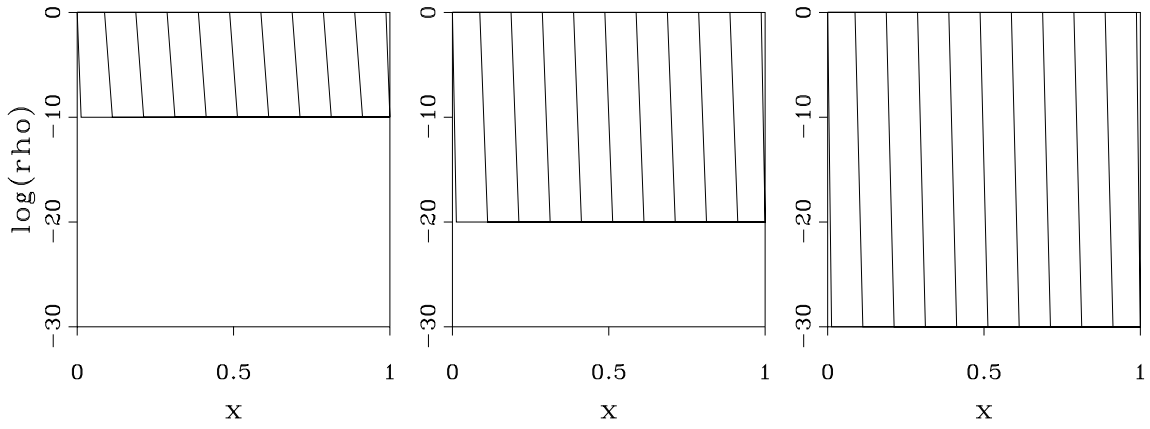

a. $\frac{\rho_w}{\rho_a} = 10^{10}$ b. $\frac{\rho_w}{\rho_a} = 10^{20}$ c. $\frac{\rho_w}{\rho_a} = 10^{30}$

Figure 9: Bulk-density profiles at $t = 0.0, 0.1, 0.2, \ldots, 1.0$, ghost-fluid method, extremely high density ratios, $h = \frac{1}{40}$.

4.1.5 Results ghost-fluid method The fix proposed in Section 3.3 is skipped, its expected smearing of the density excludes it as an interesting option here. The ghost-fluid method described in Section 3.4 *is* interesting; it works (Figure 8). For the problem at hand, it even works for arbitrarily large density ratios (Figure 9).

4.2 Oscillating water column

4.2.1 Analysis Although the previous constant-speed-and-pressure test case is not trivial from a numerical point of view, from a physical perspective it is. As a second test case we propose the following, physically more interesting one. Consider a 1D tubular circuit with a valve in it which for $t < 0$ is in open position. The tube contains a water and air column (Figure 10), flowing (for $t < 0$) at constant speed U and pressure P.

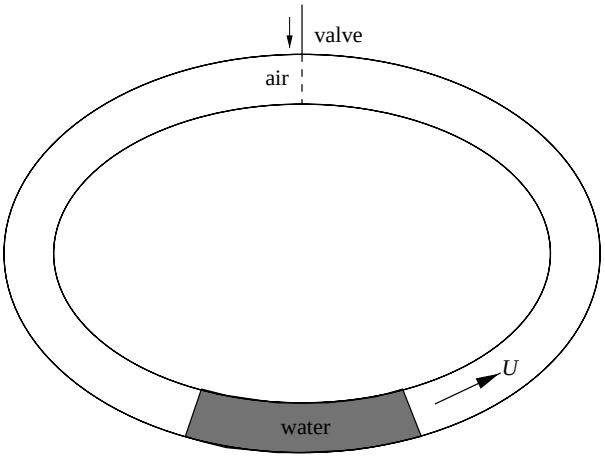

Figure 10: Tubular circuit with columns of water and air flowing at constant speed U and pressure P.

At $t = 0$, when the water column's center of gravity is at the maximum distance from the valve, the latter is instantaneously closed. Ignoring curvilinearity, the initial situation is as sketched in Figure 11. Then, starting from $t = 0$, the air at the right will be compressed by the water and the air at

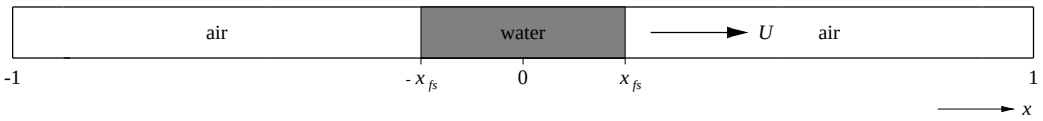

Figure 11: Initial condition: shut off tube with column of water in between two columns of air, all three columns flowing to the right at constant speed U and pressure P.

the left will expand. Hence, a pressure difference is built up across the column of water, with as a consequence a deceleration of the latter's flow to the right, followed by a stagnation, and next an acceleration and flow to the left. The latter leads to a reverse pressure gradient across the water, which will redirect the flow from left to right again, and so on. The water column starts to oscillate. An elementary analytical flow solution can be derived by making three simplifying assumptions. The first is that the density in the two air columns depends on time t only (not on the spatial coordinate x). Then, denoting the displacement of the water column in positive x-direction by $s(t)$, the density in the left and right air columns can be approximated as

$$\rho_a^l(t) = \frac{1 - x_{fs}}{1 - x_{fs} + s(t)} \rho_a(0) \quad \text{and} \tag{4.3a}$$

$$\rho_a^r(t) = \frac{1 - x_{fs}}{1 - x_{fs} - s(t)} \rho_a(0), \tag{4.3b}$$

respectively. With the equation of state, for the pressure in the two air columns it then follows:

$$p^l(t) = \left(\frac{1 - x_{fs}}{1 - x_{fs} + s(t)} \right)^{\gamma_a} P, \tag{4.4a}$$

$$p^r(t) = \left(\frac{1 - x_{fs}}{1 - x_{fs} - s(t)} \right)^{\gamma_a} P. \tag{4.4b}$$

The second assumption is that the water column behaves as a rigid body (as an ice cube say). With this, Newton's second law of motion applied to the water column's motion reads

$$\rho_w 2 x_{fs} \frac{d^2 s}{dt^2} = p^l(t) - p^r(t), \tag{4.5}$$

which, with (4.4a) and (4.4b), yields as differential equation for $s(t)$:

$$\rho_w 2 x_{fs} \frac{d^2 s}{dt^2} = \left(\left(\frac{1 - x_{fs}}{1 - x_{fs} + s(t)} \right)^{\gamma_a} - \left(\frac{1 - x_{fs}}{1 - x_{fs} - s(t)} \right)^{\gamma_a} \right) P. \tag{4.6}$$

The third assumption made is that the water column's displacements are small with respect to the length of the initial air columns: $|s(t)| \ll 1 - x_{fs}$. With this, the pressure expressions (4.4a) and (4.4b), and hence the nonlinear differential differential equation (4.6), can be linearized by good approximation:

$$\frac{d^2 s}{dt^2} + \alpha s = 0, \quad \alpha = \frac{\gamma_a P}{\rho_w x_{fs} (1 - x_{fs})}. \tag{4.7}$$

With the initial conditions $s(0) = 0$ and $\frac{ds(0)}{dt} = U$, the solution of (4.7) is

$$s(t) = \frac{U}{\sqrt{\alpha}} \sin \sqrt{\alpha} t; \tag{4.8}$$

the water column makes a harmonic oscillation with amplitude $\frac{U}{\sqrt{\alpha}}$ and oscillation time $\tau = \frac{2\pi}{\sqrt{\alpha}}$. The assumption that the pressure in the air columns is space-independent is satisfied by good approximation if $c_a \tau \gg 1 - x_{fs}$, i.e., if

$$2\pi \sqrt{\frac{x_{fs}}{1 - x_{fs}} \frac{\rho_w}{\rho_a(P)}} \gg 1. \tag{4.9a}$$

The small-displacement assumption $|s(t)| \ll 1 - x_{fs}$ implies

$$\frac{U}{c_a(P)} \sqrt{\frac{x_{fs}}{1 - x_{fs}} \frac{\rho_w}{\rho_a(P)}} \ll 1. \tag{4.9b}$$

Requirements (4.9a) and (4.9b) conflict easily. Assuming that (4.9a) is satisfied, (4.9b) can only be satisfied if $\frac{U}{c_a(P)} \ll 1$. With the linearized versions of pressure relations (4.4a) and (4.4b), for the pressure coefficients $\mathcal{P}^l \equiv \frac{p^l(t) - P}{P}$ and $\mathcal{P}^r \equiv \frac{p^r(t) - P}{P}$, it holds

$$\mathcal{P}^l(t) = -\gamma_a \frac{s(t)}{1 - x_{fs}}, \tag{4.10a}$$

$$\mathcal{P}^r(t) = \gamma_a \frac{s(t)}{1 - x_{fs}}. \tag{4.10b}$$

The two coefficients are exactly opposite in phase.

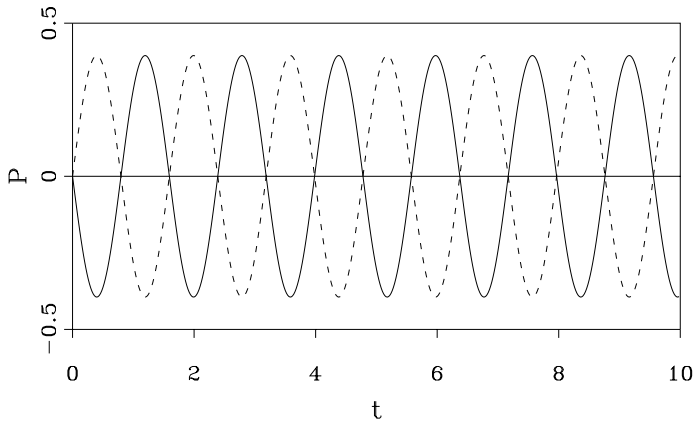

a. According to analysis

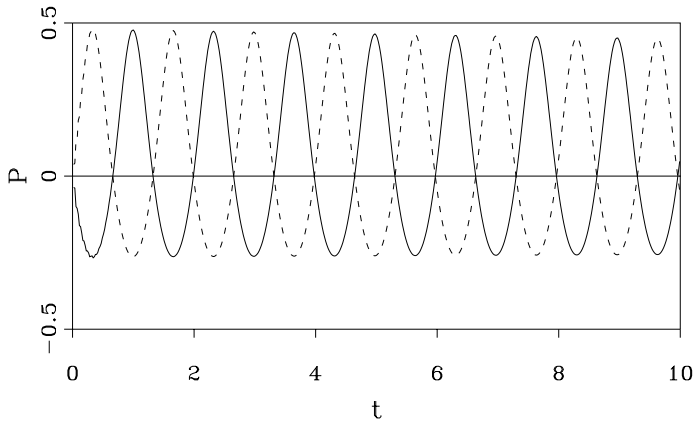

b. According to numerical computations, $h = \frac{1}{40}$.

Figure 12: Time evolution of pressure coefficients at left and right boundary (solid lines: left boundary, dashed lines: right boundary).

4.2.2 Numerics We proceed by presenting numerical results obtained through the ghost-fluid method. In the numerical computations, both water and air are taken compressible. As for the previous test case, we take $\gamma_w = 7$, $\gamma_a = \frac{7}{5}$, $B_w = 3000$, $B_a = 0$, $\rho_w(P) = 1$ and $\rho_a(P) = 0.001$. Further, we take $U = 1$, $P = 1$ and $x_{fs} = 0.1$. For these numerical choices, in Figure 12a we first give the time evolution of $\mathcal{P}^l$ and $\mathcal{P}^r$ according to the analytical estimates (4.10a) and (4.10b). For the numerical computations, an equidistant grid with $h = \frac{1}{40}$ is applied. Time integration is done again with the forward Euler scheme and the space discretization is again first-order accurate. The level-set function is taken as the signed-distance function. For this test case, as opposed to the foregoing, the level-set function is reinitialized. (The reinitialization is done after each time step.) In Figure 12b the time evolution of the pressure coefficients $\mathcal{P}(x = -1, t) = \frac{p(x=-1,t)-P}{P}$ and $\mathcal{P}(x = 1, t) = \frac{p(x=1,t)-P}{P}$ is given. Note that although requirement (4.9b) is not satisfied very well for the aforementioned numerical values, the analytical results depicted in Figure 12a still agree fairly well with the nonlinear numerical results. Also for this test case, the ghost-fluid method appears to work fine. In the ghost cells, the conservation laws are applied to virtual (ghost) amounts of water and air, not to the real physical amounts. So,

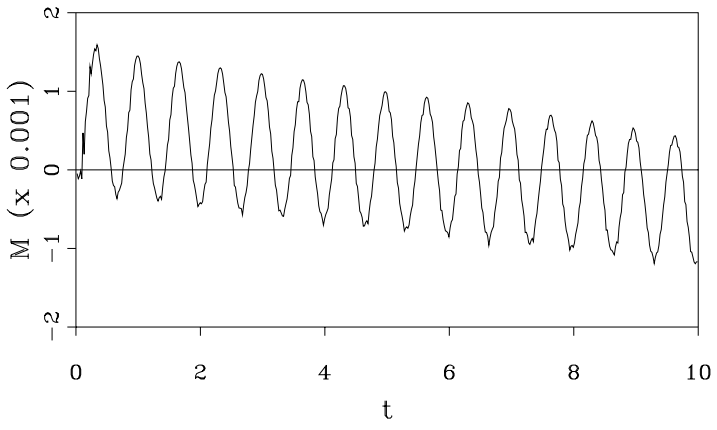

a. $h = \frac{1}{40}$

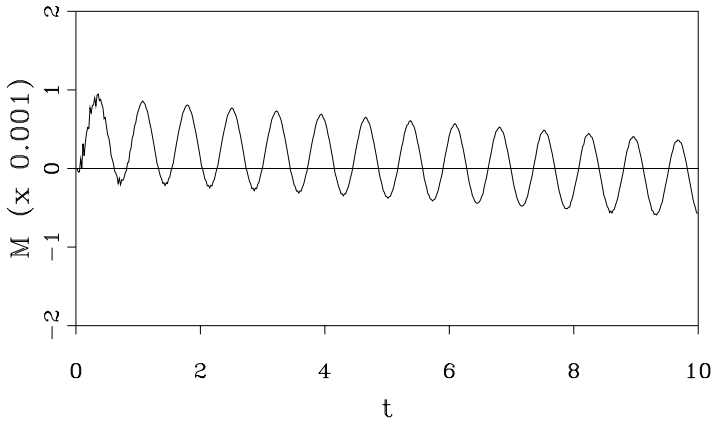

b. $h = \frac{1}{80}$

Figure 13: Time evolution of relative error in total mass of air in shut off tube.

conservation of the real amounts of mass and momentum is not guaranteed automatically. In case of accurate resolution of the level-set function and the pressure, in and near the ghost cell(s), mass and momentum are expected to be accurately conserved though (*not* exactly). In Figure 13a we give the time evolution of the relative mass error $\mathcal{M}(t) \equiv \frac{m_a(t)-m_a(0)}{m_a(0)}$, where $m_a(t)$ is the total mass of air in the shut off tube at time t. The mass error appears to be composed of two components: one oscillating and the other behaving linearly in time. Both obey the numerical method's order of accuracy, which is $\mathcal{O}(\Delta t, \Delta x)$ here. To show the latter, in Figure 13b the time evolution of the relative mass error is given for a grid and time step twice as fine as those corresponding with Figure 13a. Both the oscillation's amplitude and the linear behavior's slope appear to been halved approximately. Due to the still relatively coarse resolution of the water column (8 and 16 cells, respectively), the mass error for water (not given) does not yet show asymptotic first-order convergence behavior.

5. Conclusions

To avoid large solution errors near interfaces (an intrinsic problem of capturing methods), four fixes have been proposed, three consisting of some locally non-conservative solution update and as the fourth

a ghost-fluid fix. For density ratios of the order 1000 (typical water-air ratio) the non-conservative fixes fail, in the analyses as well as in the numerical experiments. As opposed to that, the ghost-fluid technique works. Even the computation of fronts running into vacuum ($\frac{\rho_w}{\rho_a} = \infty$) is expected to be possible with the ghost-fluid method. (Since in the ghost-fluid method only single-fluid fluxes are computed, it does not need a two-fluid Godunov approach.) The first numerical computations performed with the discretization method are promising. Extensions to higher dimensions, higher accuracy, flows with gravity, etc. are challenging. The test case performed with the oscillating water column suggests that the method may lend itself particularly well for applications as, e.g., the impact of storm surges on ships and off- and onshore constructions. Compressibility plays an important role in these problems.

References

1. S. Karni, Multicomponent flow calculations by a consistent primitive algorithm, *J. Comput. Phys.*, **112**, 31–43 (1994).
2. S. Karni, Hybrid multifluid algorithms, *SIAM J. Sci. Comput.*, **17**, 1019–1039 (1996).
3. R. Abgrall, How to prevent pressure oscillations in multicomponent flow calculations: a quasi conservative approach, *J. Comput. Phys.*, **125**, 150–160 (1996).
4. R. Abgrall and S. Karni, Computation of compressible multifluids, *J. Comput. Phys.*, **169**, 594–623 (2001).
5. M. Sussman, P. Smereka and S. Osher, A level set approach for computing solutions to incompressible two-phase flow, *J. Comput. Phys.*, **114**, 146–159 (1994).
6. R.P. Fedkiw, T. Aslam, B. Merriman and S. Osher, A non-oscillatory Eulerian approach to interfaces in multimaterial flows (the ghost fluid method), *J. Comput. Phys.*, **152**, 457–492 (1999).
7. P. Jenny, B. Müller and H. Thomann, Correction of conservative Euler solvers for gas mixtures, *J. Comput. Phys.*, **132**, 91–107 (1997).
8. B. Koren, M.R. Lewis, E.H. van Brummelen and B. van Leer, Riemann-problem and level-set approaches for two-fluid flow computations I. Linearized Godunov scheme *Report MAS-R0112*, CWI, Amsterdam (2001).

Table of Contents

1 Introduction . . . 1
2 Error near interface . . . 2
2.1 Fluid-flow equations . . . 2
2.2 Analysis for model flow . . . 2
2.3 Guidelines for error improvements . . . 4
2.3.1 Error analysis of bulk-density relation . . . 4
2.3.2 Reconsideration of fluid-flow equations near interface . . . 5
3 Fixes for error in cell with interface . . . 5
3.1 Advection of level-set function . . . 5
3.2 Advection of velocity, pressure and level-set function . . . 6
3.3 Advection of density and volume-of-fluid fraction . . . 6
3.4 Ghost-fluid method . . . 6
4 Numerical results . . . 8
4.1 Water front at constant speed and pressure . . . 8
4.1.1 Numerical choices . . . 8
4.1.2 Results fully conservative approach . . . 8
4.1.3 Results advection of level-set function . . . 8
4.1.4 Results advection of velocity, pressure and level-set function . . . 8
4.1.5 Results ghost-fluid method . . . 12
4.2 Oscillating water column . . . 12
4.2.1 Analysis . . . 12
4.2.2 Numerics . . . 14
5 Conclusions . . . 15
References . . . 17